Article

Characterization of Self-Assembled Monolayers of Porphyrins Bearing Multiple Thiol-Derivatized Rigid-Rod Tethers

Amir A. Yasseri, Dennis Syomin, Vladimir L. Malinovskii, Robert S. Loewe, Jonathan S. Lindsey, Francisco Zaera, and David F. Bocian

J. Am. Chem. Soc., **2004**, 126 (38), 11944-11953• DOI: 10.1021/ja047723t • Publication Date (Web): 31 August 2004

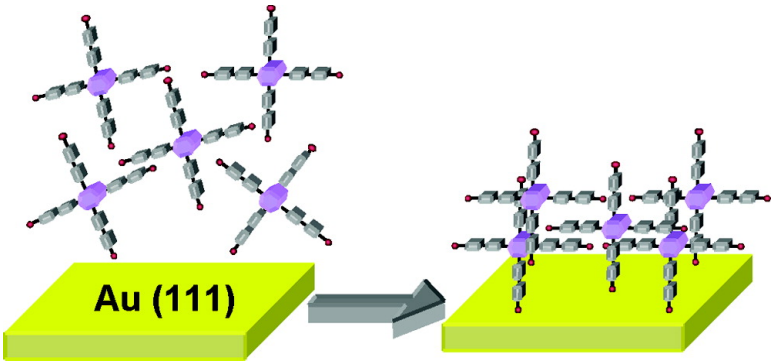

More About This Article

Additional resources and features associated with this article are available within the HTML version:

- Supporting Information
- Links to the 7 articles that cite this article, as of the time of this article download
- Access to high resolution figures
- Links to articles and content related to this article
- Copyright permission to reproduce figures and/or text from this article

View the Full Text HTML

J|A|C|S
ARTICLES
Published on Web 08/31/2004

Characterization of Self-Assembled Monolayers of Porphyrins Bearing Multiple Thiol-Derivatized Rigid-Rod Tethers

Amir A. Yasseri,[†] Dennis Syomin,[†] Vladimir L. Malinovskii,[‡] Robert S. Loewe,[‡] Jonathan S. Lindsey,*[,‡] Francisco Zaera,*[,†] and David F. Bocian*[,†]

Contribution from the Department of Chemistry, University of California, Riverside, California 92521-0403, and Department of Chemistry, North Carolina State University, Raleigh, North Carolina 27695-8204

Received April 20, 2004; E-mail: jlindsey@ncsu.edu; francisco.zaera@ucr.edu; david.bocian@ucr.edu

Abstract: A series of multithiol-functionalized zinc porphyrins has been prepared and characterized as self-assembled monolayers (SAMs) on Au. The molecules, designated **ZnPS$_n$** (n = 1−4), contain from one to four [(*S*-acetylthio)methyl]phenylethynylphenyl groups appended to the *meso*-position of the porphyrin; the other *meso*-substituents are phenyl groups. For the dithiol-functionalized molecules, both the *cis*- and the *trans*-appended structures were examined. The **ZnPS$_n$** SAMs were investigated using X-ray photoelectron spectroscopy, Fourier transform infrared spectroscopy, and various electrochemical methods. The studies reveal the following characteristics of the **ZnPS$_n$** SAMs. (1) The **ZnPS$_n$** molecules bind to the Au surface via a single thiol regardless of the number of thiol appendages that are available per molecular unit. (2) The porphyrins in the **ZnPS$_3$** and **ZnPS$_4$** SAMs bind to the surface in a more upright orientation than the porphyrins in the **ZnPS$_1$**, *cis*-**ZnPS$_2$**, and *trans*-**ZnPS$_2$** SAMs. The porphyrins in the **ZnPS$_3$** and **ZnPS$_4$** SAMs are also more densely packed than those in the *cis*-**ZnPS$_2$** and *trans*-**ZnPS$_2$** SAMs. The packing density of the **ZnPS$_3$** and **ZnPS$_4$** SAMs is similar to that of the **ZnPS$_1$** SAMs, despite the larger size of the molecules in the former SAMs. (3) The thermodynamics and kinetics of electron transfer are generally similar for all of the **ZnPS$_n$** SAMs. The general similarities in the electron-transfer characteristics for all of the SAMs are attributed to the similar binding motif.

I. Introduction

Self-assembled monolayers (SAMs) of thiol-derivatized molecules on Au substrates have been widely studied in connection with their potential applications in the general area of molecular-based electronics.[1,2] Molecules have been designed to be tethered to the Au substrate via one or more thiols, including tripodal units bearing three thiols.[3−11] Molecules also have been constructed with two thiols at opposite ends, thus affording the opportunity of spanning two different metal electrodes and establishing direct electrical contact to both.[12−14] In this regard, dithiol-functionalized molecules have been implemented in a variety of two-terminal devices to explore phenomena related to molecular electronics, including conductance switching in nanopores,[15−17] and resonant tunneling behavior in break junctions.[18]

We have been engaged in a program aimed at constructing devices that use the redox properties of porphyrinic molecules to store information.[14,19−22] In the course of these studies, we

[†] University of California, Riverside.
[‡] North Carolina State University.

(1) Kwok, K. S.; Ellenbogen, J. C. *Mater. Today* **2002**, *5*, 28−37.
(2) Carroll, R. L.; Gorman, C. B. *Angew. Chem., Int. Ed.* **2002**, *41*, 4378−4400.
(3) Whitesell, J. K.; Chang, H. K. *Science* **1993**, *261*, 73−76.
(4) Fox, M. A.; Whitesell, J. K.; McKerrow, A. J. *Langmuir* **1998**, *14*, 816−820.
(5) Fox, M. A.; Li, W.; Wooton, M.; McKerrow, A.; Whitesell, J. K. *Thin Solid Films* **1998**, *327−329*, 477−480.
(6) Siiman, O.; Burshteyn, A.; Maples, J. A.; Whitesell, J. K. *Bioconjugate Chem.* **2000**, *11*, 549−556.
(7) Zhu, L.; Tang, H.; Harima, Y.; Yamashita, K.; Hirayama, D.; Aso, Y.; Otsubo, T. *Chem. Commun.* **2001**, 1830−1831.
(8) Kittredge, K. W.; Minton, M. A.; Fox, M. A.; Whitesell, J. K. *Helv. Chim. Acta* **2002**, *85*, 788−798.
(9) Zhu, L.; Tang, H.; Harima, Y.; Yamashita, K.; Aso, Y.; Otsubo, T. *J. Mater. Chem.* **2002**, *12*, 2250−2254.
(10) Hirayama, D.; Takimiya, K.; Aso, Y.; Otsubo, T.; Hasobe, T.; Yamada, H.; Imahori, H.; Fukuzumi, S.; Sakata, Y. *J. Am. Chem. Soc.* **2002**, *124*, 532−533.
(11) Wei, L.; Padmaja, K.; Youngblood, W. J.; Lysenko, A. B.; Lindsey, J. S.; Bocian, D. F. *J. Org. Chem.* **2004**, *69*, 1461−1469.
(12) Jagessar, R. C.; Tour, J. M. *Org. Lett.* **2000**, *2*, 111−113.
(13) Tour, J. M.; Jones, L., II; Pearson, D. L.; Lamba, J. J. S.; Burgin, T. P.; Whitesides, G. M.; Allara, D. L.; Parikh, A. N.; Atre, S. V. *J. Am. Chem. Soc.* **1995**, *117*, 9529−9534.
(14) Schweikart, K.-H.; Malinovskii, V. L.; Yasseri, A. A.; Li, J.; Lysenko, A. B.; Bocian, D. F.; Lindsey, J. S. *Inorg. Chem.* **2003**, *42*, 7431−7446.
(15) Chen, J.; Wang, W.; Klemic, J.; Reed, M. A.; Axelrod, B. W.; Kaschak, D. M.; Rawlett, A. M.; Price, D. W.; Dirk, S. M.; Tour, J. M.; Grubisha, D. S.; Bennett, D. W. *Ann. N.Y. Acad. Sci.* **2002**, *960*, 69−99.
(16) Chen, J.; Wang, W.; Reed, M. A.; Rawlett, A. M.; Price, D. W.; Tour, J. M. *Appl. Phys. Lett.* **2000**, *77*, 1224−1226.
(17) Donhauser, Z. J.; Mantooth, B. A.; Kelly, K. F.; Bumm, L. A.; Monnell, J. D.; Stapleton, J. J.; Price, D. W. J.; Rawlett, A. M.; Allara, D. L.; Tour, J. M.; Weiss, P. S. *Science* **2001**, *292*, 2303−2307.
(18) Reichert, J.; Ochs, R.; Beckmann, D.; Weber, H. B.; Mayor, M.; Lohneysen, H. V. *Phys. Rev. Lett.* **2002**, *88*, 176804/1−176804/4.
(19) Balakumar, A.; Lysenko, A. B.; Carcel, C.; Malinovskii, V. L.; Gryko, D. T.; Schweikart, K.-H.; Loewe, R. S.; Yasseri, A. A.; Liu, Z.; Bocian, D. F.; Lindsey, J. S. *J. Org. Chem.* **2004**, *69*, 1435−1443.
(20) Schweikart, K.-H.; Malinovskii, V. L.; Diers, J. R.; Yasseri, A. A.; Bocian, D. F.; Kuhr, W. G.; Lindsey, J. S. *J. Mater. Chem.* **2002**, *12*, 808−828.
(21) Gryko, D.; Li, J.; Diers, J. R.; Roth, K. M.; Bocian, D. F.; Kuhr, W. G.; Lindsey, J. S. *J. Mater. Chem.* **2001**, *11*, 1162−1180.
(22) Gryko, D. T.; Clausen, C.; Roth, K. M.; Dontha, N.; Bocian, D. F.; Kuhr, W. G.; Lindsey, J. S. *J. Org. Chem.* **2000**, *65*, 7345−7355.

10.1021/ja047723t CCC: $27.50

have designed and synthesized a wide variety of porphyrinic architectures and characterized their self-assembly behavior both on metal and on semiconductor surfaces. We have also extensively probed the kinetics of interfacial charge transfer in the porphyrinic SAMs.[23−26] To date, our studies of porphyrin-based information storage media have focused on architectures that are tethered to one electroactive surface. The electrical contact to the second electrode is noncovalent in nature and is typically established through an intervening conductive medium.

To expand on our capabilities for the design of electronic devices at the molecular level, we have embarked on a program to explore porphyrinic architectures in which the molecules contain multiple functional groups for surface attachment. A number of previous studies have been reported of multi-thiol-functionalized porphyrin SAMs,[11,27−38] prepared for a variety of applications including nanopatterning for optical chemical sensing, molecular biorecognition,[28−35] and electrocatalytic oxygen reduction.[36−38] However, these previous studies have typically used a single type of multithiol-functionalized porphyrin and have not explored how the number and location of the thiol groups might affect the mode of surface binding and geometry, or how these factors might influence the desired functional characteristics.

In this paper, we report the preparation and characterization of a series of multithiol-functionalized zinc porphyrin SAMs on Au. These molecules, designated **ZnPS*n*** ($n = 1-4$), contain from one to four [(*S*-acetylthio)methyl]phenylethynylphenyl groups appended to the *meso*-position of the porphyrin, the other *meso*-substituents being phenyl groups (Chart 1). For the dithiol-functionalized molecules, both the *cis*- and the *trans*-appended structures were examined. The *S*-acetyl protecting group undergoes facile cleavage upon exposure to the Au surface, leaving an unprotected sulfur atom that binds directly to the Au surface.[13] For convenience, we will refer to the protected and unprotected appendages as ***S*-AcSCH$_2$pep** and **SCH$_2$pep**, respectively. The ***S*-AcSCH$_2$pep** functionalization was chosen because this group is relatively rigid, which is expected to disfavor surface orientations where the porphyrin rings lay flat or close to flat on the surface. Indeed, previous studies of molecular SAMs based on similar rodlike designs have shown that these molecules form highly ordered densely packed monolayers,[39,40] wherein the molecules align themselves in upright orientations on the surface.[40] A similar surface orientation for the multithiol-functionalized porphyrins (e.g., *trans*-**ZnPS$_2$**) could, in principle, allow the molecule to span two metal electrodes and make direct electrical contact to both. Porphyrins with *cis*-thiol functionalization (i.e., *cis*-**ZnPS$_2$**, **ZnPS$_3$**, and **ZnPS$_4$**) were included in the study to explore whether this would afford binding to a given surface via two adjacent thiol groups. Attachment via two thiols could afford enhanced stability and

Chart 1

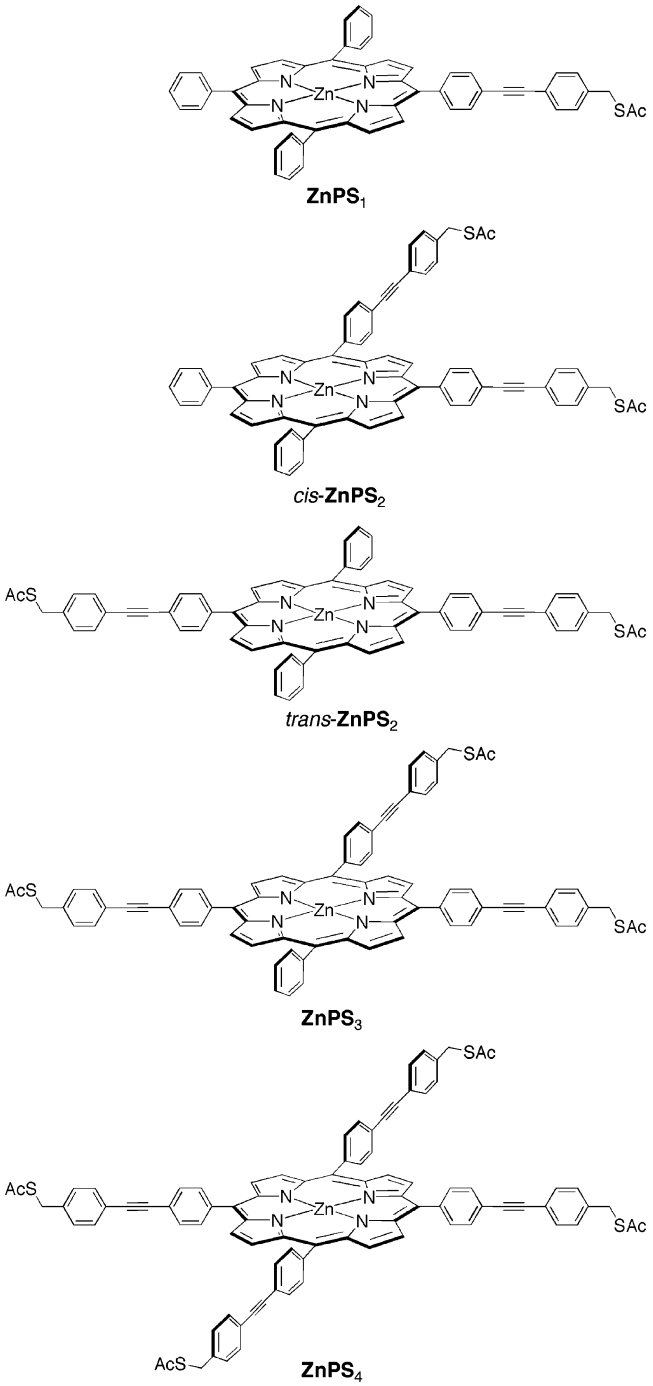

(23) Roth, K. M.; Liu, Z.; Gryko, D. T.; Clausen, C.; Lindsey, J. S.; Bocian, D. F.; Kuhr, W. G. *ACS Symp. Ser.* **2003**, *844*, 51−61.
(24) Roth, K. M.; Lindsey, J. S.; Bocian, D. F.; Kuhr, W. G. *Langmuir* **2002**, *18*, 4030−4040.
(25) Roth, K. M.; Gryko, D. T.; Clausen, C.; Li, J.; Lindsey, J. S.; Kuhr, W. G.; Bocian, D. F. *J. Phys. Chem. B* **2002**, *106*, 8639−8648.
(26) Roth, K. M.; Dontha, N.; Dabke, R. B.; Gryko, D. T.; Clausen, C.; Lindsey, J. S.; Bocian, D. F.; Kuhr, W. G. *J. Vac. Sci. Technol., B* **2000**, *18*, 2359−2364.
(27) Tomizaki, K.-y.; Yu, L.; Wei, L.; Bocian, D. F.; Lindsey, J. S. *J. Org. Chem.* **2003**, *68*, 8199−8207.
(28) Boeckl, M. S.; Bramblett, A. L.; Hauch, K. D.; Sasaki, T.; Ratner, B. D.; Rogers, J. W., Jr. *Langmuir* **2000**, *16*, 5644−5653.
(29) Shimazu, K.; Takechi, M.; Fujii, H.; Suzuki, M.; Saiki, H.; Yoshimura, T.; Uosaki, K. *Thin Solid Films* **1996**, *273*, 250−253.
(30) Ishida, A.; Sakata, Y.; Majima, T. *Chem. Commun.* **1998**, 57−58.
(31) Ishida, A.; Sakata, Y.; Majima, T. *Chem. Lett.* **1998**, 267−268.
(32) Akiyama, T.; Imahori, H.; Sakata, Y. *Chem. Lett.* **1994**, 1447−1450.
(33) Cordas, C. M.; Viana, A. S.; Leupold, S.; Montforts, F.-P.; Abrantes, L. M. *Electrochem. Commun.* **2003**, *5*, 36−41.
(34) Kondo, T.; Ito, T.; Nomura, S.-I.; Uosaki, K. *Thin Solid Films* **1996**, *284−285*, 652−655.
(35) Zhang, Z.; Hu, R.; Liu, Z. *Langmuir* **2000**, *16*, 1158−1162.
(36) Hutchison, J. E.; Postlethwaite, T. A.; Murray, R. W. *Langmuir* **1993**, *9*, 3277−3283.
(37) Zak, J.; Yuan, H.; Ho, M.; Woo, L. K.; Porter, M. D. *Langmuir* **1993**, *9*, 2772−2774.
(38) Van Galen, D. A.; Majda, M. *Anal. Chem.* **1988**, *60*, 1549−1553.
(39) Walzer, K.; Marx, E.; Greenham, N. C.; Less, R. J.; Raithby, P. R.; Stokbro, K. *J. Am. Chem. Soc.* **2004**, *126*, 1229−1234.
(40) Dhirani, A.-A.; Zehner, R. W.; Hsung, R. P.; Guyot-Sionnest, P.; Sita, L. R. *J. Am. Chem. Soc.* **1996**, *118*, 3319−3320.

might also alter the electron-transfer properties from those of a single-thiol attached species.[14,25]

The series of **ZnPS$_n$** SAMs on Au mentioned above was investigated using a variety of techniques, including X-ray photoelectron spectroscopy (XPS), Fourier transform infrared (FTIR) spectroscopy, and various electrochemical methods (cyclic voltammetry, swept-waveform AC voltammetry (SWAV), and open circuit potential amperometry (OCPA)). The XPS studies were used to elucidate the details of the surface bonding. The voltammetric and FTIR studies were used to provide information on packing density and surface orientation, respectively. The SWAV and OCPA measurements were used to obtain the rates of charge transfer in the presence of applied potential and the rate of charge dissipation in the absence of applied potential. Collectively, the studies reported herein provide a detailed picture of the structural and functional characteristics of the porphyrin SAMs and demonstrate how these characteristics vary with the number of ***S*-AcSCH$_2$pep** appendages.

II. Experimental Section

A. Synthesis. The synthesis of the porphyrins is reported in the Supporting Information.

B. Au Substrate Fabrication. 1. Microelectrodes for Electrochemical Studies. Both Au ball and band microelectrodes were used for the electrochemical studies. These electrodes were prepared according to previously described methods.[24,41] Microelectrodes are required for the measurement of the electron-transfer rates to ensure that the RC time constant of the electrochemical cell does not limit the measurement. The Au ball microelectrodes have the advantage of ease of use. However, the surface morphology and geometry of these electrodes are different from those of the Au band microelectrodes, which are more similar to the larger area Au films required for the spectroscopic studies. Initial studies aimed at comparing the properties (redox potentials, surface coverages) of the porphyrin SAMs on the Au ball with those of the band microelectrodes indicated little difference between the two. Consequently, further electrochemical studies used the Au ball microelectrodes.

2. Evaporated Films for Spectroscopic Studies. Au films were used as substrates for the XPS and FTIR studies. The films were prepared by e-beam vapor deposition of 10 nm of Cr (99.999%) followed by 200 nm of Au (99.99%) onto the surface of a precleaned oxidized B-doped Si (100) wafer (Silicon Valley Microelectronics). The Cr and Au films were deposited at 0.5 and 1.5 Å s^{-1}, respectively. The base pressure of the chamber during the evaporation period was maintained at $<2.0 \times 10^{-6}$ Torr. Upon completion of the film deposition, the wafer was removed from vacuum and diced into ~1 cm^2 pieces. Each Au piece was immediately inserted into a VOC-type glass vial fitted with a Teflon-silicon rubber septum (ambient exposure of ~5−10 min). The vial was purged with Ar (99.995%) to maintain the sample under an inert environment. XPS survey spectra revealed no noticeable differences in the level of carbon contamination between Au samples used immediately and those stored under Ar for a few days. However, to maintain self-consistency in all surface characterization and electrochemical experiments, fresh Au substrates were used immediately after preparation.

C. SAM Preparation. The SAMs were prepared from porphyrins in CH_2Cl_2:EtOH (85:15) solutions. The mixed solvent was used because of the low solubility of the porphyrins containing multiple ***S*-AcSCH$_2$pep** appendages. The surface coverage and the conditions required for achieving saturation coverage were determined electrochemically in a series of experiments wherein the concentration of the porphyrin in the deposition solution and the deposition time were systematically varied. These experiments revealed that the surface coverage could be varied in a controlled fashion from the low 10^{-12} to mid 10^{-11} mol cm^{-2} range by varying the porphyrin concentration from ~3 μM to ~3 mM and the deposition time from 1 to 15 min. Saturation coverages, which fall in the mid 10^{-11} mol cm^{-2} range for all of the porphyrins, could be achieved by deposition from 3 mM solutions for 15 min.

Saturation-coverage SAMs for the electrochemical studies were prepared by immersing the Au microelectrodes in a ~3 mM porphyrin solution for ~15 min, followed by repeated (five times) sonication and rinsing with CH_2Cl_2. Saturation-coverage SAMs for the XPS and FTIR studies were prepared by depositing successive 50 μL aliquots of a 3 mM porphyrin solution onto the Au substrate, which was presealed in a vial purged with Ar. After ~15 min, the vial was opened and the substrate was repeatedly sonicated and rinsed (five times) with CH_2Cl_2, sealed once again in the vial, and dried with a stream of Ar. The SAMs were kept under Ar with minimum exposure to light prior to the XPS and FTIR measurements. The SAMs prepared at less than saturation coverage for the electrochemical and FTIR experiments were obtained by procedures similar to those described above, except for the use of different concentrations of the porphyrin solution and deposition times, chosen to achieve the desired surface coverage.

D. Electrochemical Measurements. The electrochemical measurements on the porphyrins in solution and SAMs were made using a Pt wire or Au micro working electrode, respectively, a Pt counter electrode, and a Ag reference electrode. The solvent was CH_2Cl_2:EtOH (85:15); the supporting electrolyte was 1.0 M Bu_4NPF_6 (Aldrich), recrystallized three times from methanol (Fisher) and dried overnight at room temperature under vacuum. The RC time constant for the microelectrode/electrochemical cell was measured to be ~5 μs, which is sufficiently short to preclude interference with the measurement of the electron-transfer rates.

1. Voltammetric Characterization. Cyclic voltammograms were recorded in a 0−1.2 V potential window with a CH Instruments Electrochemical Analyzer (model 600A). For the SAMs, the charge obtained by integrating the first anodic voltammetric peak was used to determine the surface coverage. The area of the working electrode was determined after the electrochemical measurement on each SAM. The SAM was first stripped from the electrode by immersing in Nanostrip solution (J. T. Baker) for 5 min followed by rinsing of the electrode. The cleaned electrode was then placed in a 1 mM ferrocene solution (CH_2Cl_2:EtOH (85:15) containing 1.0 M Bu_4NPF_6), and the voltammetric signal observed at 1 V s^{-1} was used to obtain the electrode area via the Randles−Sevcik equation.[42] The half-wave potential ($E_{1/2}$) obtained for ferrocene in this electrochemical configuration is $E_{1/2} \approx$ 0.20 V, which serves as a reference point for the potentials of the SAMs.

2. Determination of Electron-Transfer Rates. The standard electron-transfer rate constants (k^0) of the SAMs were obtained using the swept waveform AC voltammetry (SWAV) method. This method has been described in detail previously, and its utility has been demonstrated for obtaining kinetic data for porphyrin SAMs.[25] The current observed in the SWAV measurement was collected and amplified by a homemade broad bandwidth amplifier (3db point 450 kHz).

3. Determination of Charge-Retention Times. The charge-retention characteristics of the SAMs were determined using open circuit potential amperometry (OCPA) as described in detail in past publications.[24,26,43]

E. XPS Measurements. The XPS data for the porphyrin SAMs were collected using a Leybold EA11-MCD system equipped with a Mg Kα X-ray (1253.6 eV) source, a hemispherical analyzer, and a 18-

(41) Creager, S.; Yu, C. J.; Bamdad, C.; O'Connor, S.; MacLean, T.; Lam, E.; Chong, Y.; Olsen, G. T.; Luo, J.; Gozin, M.; Kayyem, J. F. *J. Am. Chem. Soc.* **1999**, *121*, 1059−1064.

(42) Bard, A. J.; Faulkner, L. R. *Electrochemical Methods: Fundamentals and Applications*; Wiley: New York, 2001.

(43) Roth, K. M.; Yasseri, A. A.; Liu, Z.; Dabke, R. B.; Malinovskii, V.; Schweikart, K.-H.; Yu, L.; Tiznado, H.; Zaera, F.; Lindsey, J. S.; Kuhr, W. G.; Bocian, D. F. *J. Am. Chem. Soc.* **2003**, *125*, 505−517.

multichannel detector. The main XPS chamber was maintained at a base pressure of $<3 \times 10^{-8}$ Torr. The samples were introduced by using a fast-transfer mechanism comprised of a long rod and an intermediate pumping stage. The total time required for the introduction of the sample was approximately 5 min. Spectra were obtained from each sample using identical data collection parameters. The survey (scans of 1000 eV or more) and high-resolution spectra were obtained by averaging 10 or 50 scans, with an average dwell time of 100 or 250 ms per point and scan, respectively. Survey spectra were obtained with a band-pass energy of 100.8 eV, which corresponds to a spectral resolution, $\Delta E_{1/2} \approx 1.5$ eV. High-resolution spectra were obtained for the S 2p, Zn 2p, N 1s, C 1s, and O 1s lines for all of the SAMs with a band-pass energy of 31.5 eV ($\Delta E_{1/2} \approx 0.8$ eV). To compensate for energy shifts due to possible surface charging effects, all of the XPS peak positions were referenced to the adventitious C 1s peak at 284.6 eV.

The spectra from the high-resolution scans were fitted to Gaussian peaks after background subtraction (using Analytics software) for semiquantitative analysis. In the case of the S signal, 2p doublets are observed for both surface-bound and unbound species, which are not fully resolved. Consequently, the S 2p lines were fitted by setting the energy difference between the 2 $p_{3/2}$ and 2 $p_{1/2}$ peaks to 1.2 eV and their area ratio to 2:1, and by maintaining a constant peak width at half-maximum. The relative intensities and binding energies of each pair of doublets were then allowed to vary in the fitting process. The binding energies for the surface-bound S atoms for the different **ZnPS**$_n$ SAMs were found to be identical to within experimental error; only the relative intensities of the signals varied. The same was also the case for the unbound S atoms of the different **ZnPS**$_n$ SAMs. In the case of the N 1s and Zn $2p_{3/2}$ bands, the fits were constrained such that the same parameters were used for the different porphyrin SAMs.

F. FTIR Spectroscopy. The FTIR spectra of the porphyrins in both solids and SAMs were collected at room temperature using a Bruker Tensor 27 FTIR spectrometer. In all cases, the spectral resolution was 4 cm^{-1}. The spectra of the solid porphyrin samples were obtained in KBr pellets ($\sim 1-2$ wt % of porphyrin). These spectra were collected in transmission mode using a room-temperature DTGS detector and were averaged over 32 scans. The spectra of the SAMs were acquired using a Harrick Scientific horizontal single-reflection Germanium ATR accessory GATR (65° incidence angle). In the reflection accessory, the SAM on the Au substrate is placed against the Ge crystal that serves as the optical element of the GATR. A constant torque setting was used in all measurements. During the spectra acquisition period, the GATR accessory was purged with dry N_2. Before every experiment, the Ge crystal was cleaned with neat 2-butanone. The spectra of the SAMs were acquired using a liquid-nitrogen cooled medium-bandwidth MCT detector ($600-4000$ cm^{-1}) and were averaged over 256 scans. The peak-to-peak noise in the SAM spectra was $\leq 1.5 \times 10^{-4}$ absorbance units.

III. Results

A. Electrochemical Studies of the ZnPS$_n$ SAMs. 1. Voltammetric Characteristics. Representative fast scan (100 V s^{-1}) cyclic voltammograms of the saturation-coverage **ZnPS**$_n$ SAMs are presented in Figure 1. All of the SAMs exhibit robust and reversible electrochemical behavior over multiple cycles under ambient conditions. At oxidizing potentials, each SAM exhibits two resolved voltammetric waves indicative of the mono- and dication porphyrin radicals. The half-wave potentials for the different **ZnPS**$_n$ SAMs and the surface concentrations (Γ) at saturation coverage are summarized in Table 1. For comparison, redox potentials for the **ZnPS**$_n$ porphyrins in solution are included in Table 1.

Inspection of the redox data in Table 1 shows that while the solution potentials for all of the **ZnPS**$_n$ porphyrins are the same

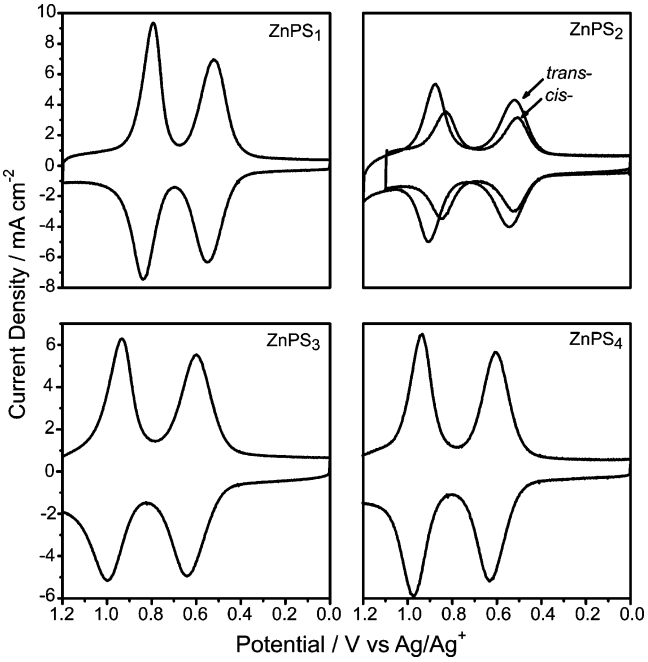

Figure 1. Representative fast-scan voltammograms (100 V s^{-1}) of saturation-coverage **ZnPS**$_n$ ($n = 1-4$) SAMs.

Table 1. Redox Potentials for Oxidation of the **ZnPS**$_n$ Porphyrins in Solution and Saturation-Coverage SAMs and Surface Concentrations for the SAMs[a]

	$E^{0/+1}$		$E^{+1/+2}$			
SAM	soln (V)	SAM (V)	soln (V)	SAM (V)	Γ[b] (10^{-11} mol cm^{-2})	area[c] Å^2
ZnPS$_1$	0.47	0.54	0.69	0.82	7.6	220
cis-**ZnPS$_2$**	0.48	0.52	0.74	0.84	3.0	550
trans-**ZnPS$_2$**	0.48	0.53	0.73	0.89	4.7	350
ZnPS$_3$	0.49	0.62	0.70	0.97	6.7	250
ZnPS$_4$	0.49	0.62	0.71	0.96	6.5	260

[a] All redox potentials were obtained in CH_2Cl_2:EtOH (85:15) containing 1.0 M *n*-Bu_4NPF_6 and were referenced vs Ag/Ag^+ ($FcCp_2/FcCp_2^+ \approx 0.19$ V). The scan rates for the solution and SAM studies were 0.1 and 100 V s^{-1}, respectively. [b] Calculated from the integrated voltammetric peaks. [c] Estimated from the experimental values of Γ.

to within experimental error, the potentials for all of the **ZnPS**$_n$ SAMs are higher than those for the porphyrins in solution. Also, the potentials for the **ZnPS$_3$** and **ZnPS$_4$** SAMs ($E^{0/+1} \approx 0.62$ V) are more positive than those for the **ZnPS$_1$**, *cis*-**ZnPS$_2$**, and *trans*-**ZnPS$_2$** SAMs ($E^{0/+1} \approx 0.53$ V). In this regard, previous studies of porphyrin SAMs have shown that the redox potentials are influenced by both packing density and screening from solvent and counterions.[25] More densely packed or heavily screened SAMs typically exhibit higher redox potentials. The fact that the **ZnPS$_3$** ($\Gamma \approx 6.7 \times 10^{-11}$ mol cm^{-2}) and **ZnPS$_4$** ($\Gamma \approx 6.5 \times 10^{-11}$ mol cm^{-2}) SAMs exhibit higher redox potentials than the *cis*-**ZnPS$_2$** ($\Gamma \approx 3.0 \times 10^{-11}$ mol cm^{-2}) or *trans*-**ZnPS$_2$** ($\Gamma \approx 4.7 \times 10^{-11}$ mol cm^{-2}) SAMs is qualitatively consistent with the result that the former porphyrins exhibit higher saturation coverages than the latter. The **ZnPS$_1$** SAM, on the other hand, does not follow the trend; this SAM exhibits a relatively low redox potential ($E^{0/+1} \approx 0.53$ V) despite the fact that the saturation surface coverage is high ($\Gamma \approx 7.6 \times 10^{-11}$ mol cm^{-2}). Plausibly, the phenyl substituents on **ZnPS$_1$**, which are much smaller than the ***S*-AcSCH$_2$pep** appendages on the other porphyrins, may be less effective at screening the

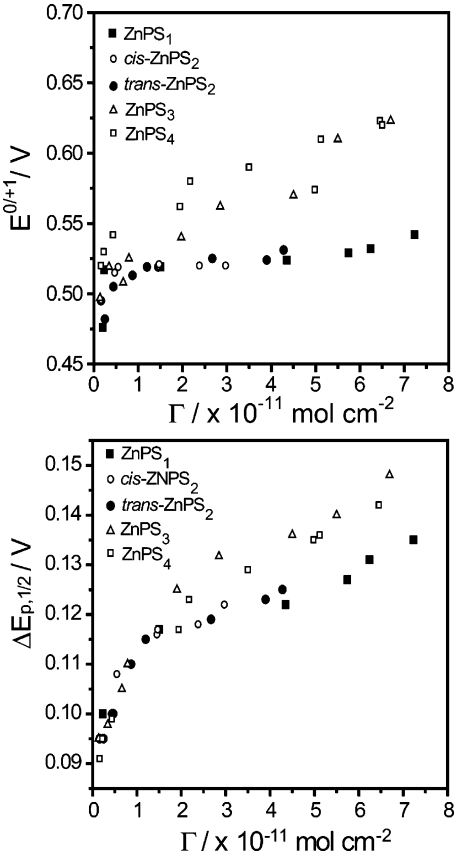

Figure 2. Redox potentials $E^{0/+1}$ (top panel) and full-width at half-maxima $\Delta E_{p,1/2}$ (anodic peak) (bottom panel) of the **ZnPS$_n$** ($n = 1-4$) SAMs at various surface concentrations.

porphyrin from the solvent and counterions, thus leading to a lower redox potential.[25]

To evaluate more fully the effects of surface concentration on the electrochemical characteristics of the SAMs, voltammetric measurements for all of the **ZnPS$_n$** SAMs were performed as a function of surface coverage. The potential for each first oxidation ($E^{0/+1}$) and full-width at half-maximum for the anodic peak of this oxidation ($\Delta E_{p,1/2}$) are plotted in Figure 2, top and bottom panels, respectively. Inspection of these data reveals the following: (1) At low surface concentrations ($\Gamma \approx 2 \times 10^{-12}$ mol cm^{-2}), the $E^{0/+1}$ values for all of the **ZnPS$_n$** SAMs are similar to one another and approach the solution value. (2) As the surface concentration increases, the $E^{0/+1}$ values increase. (3) While the $E^{0/+1}$ values for **ZnPS$_3$** and **ZnPS$_4$** continue to increase as the coverage approaches the saturation value, the $E^{0/+1}$ values for *cis*-**ZnPS$_2$** and *trans*-**ZnPS$_2$** appear to level off before saturation coverage is reached. Leveling off is clearly observed for **ZnPS$_1$**. The trends observed for the $\Delta E_{p,1/2}$ values are generally similar to those observed for the $E^{0/+1}$ values: (1) At low surface concentrations, the $\Delta E_{p,1/2}$ values for all of the **ZnPS$_n$** SAMs are similar to one another and fall in the 90−100 mV range, near the thermodynamic minimum for a redox homogeneous monolayer. (2) As the surface concentration increases, the $\Delta E_{p,1/2}$ values increase, indicative of increasing (albeit relatively small) redox heterogeneity. (3) The $\Delta E_{p,1/2}$ values for **ZnPS$_3$** and **ZnPS$_4$** continue to increase as the coverage approaches the saturation value, but the $\Delta E_{p,1/2}$ values for *cis*-**ZnPS$_2$** and *trans*-**ZnPS$_2$** appear to level off before saturation coverage is reached. Leveling off is clearly observed for **ZnPS$_1$**. Finally, we note that for all of the **ZnPS$_n$** SAMs, the peak-to-peak splitting between the anodic and cathodic waves is ~0.03 V and does not change as a function of surface coverage.

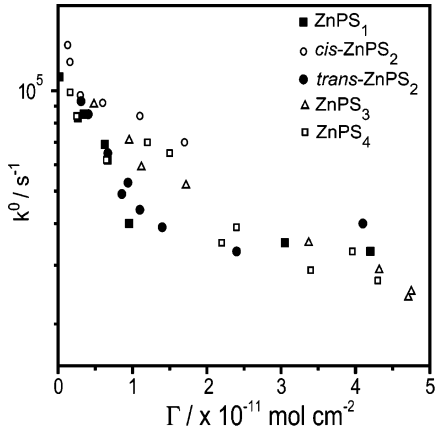

Figure 3. Plot of k^0 versus surface concentration for the $E^{0/+1}$ state of the **ZnPS$_n$** ($n = 1-4$) SAMs.

2. Electron-Transfer and Charge-Retention Characteristics. Both the standard electron-transfer rate constants, k^0, and the charge-dissipation rates (in the absence of applied potential), reported as charge-retention half-life times, $t_{1/2}$, were measured simultaneously for each of the **ZnPS$_n$** SAMs. These studies were undertaken because our previous work on porphyrin SAMs have shown that the k^0 and $t_{1/2}$ values depend on surface coverage.[25,43] The plot of k^0 for the first oxidation processes ($E^{0/+1}$) as a function of surface concentration shown for the **ZnPS$_n$** SAMs in Figure 3 indicates that, indeed, higher surface coverage results in slower rates of electron transfer; inspection of the charge-dissipation data indicates the same trend (data not shown). At low surface concentration, the k^0 values for all of the **ZnPS$_n$** SAMs are similar to one another, ~10^5 s^{-1}. As the surface concentration increases, the k^0 values decrease and appear to level off for all of the SAMs at $k^0 \approx 2 \times 10^4$ s^{-1} at a surface concentration of $\Gamma \approx 2 \times 10^{-11}$ mol cm^{-2}, well below the saturation coverage of any of the SAMs. It should be noted that the rates cannot be measured at very high surface concentrations because of limitations in the experimental apparatus. In terms of the charge-retention half-lives, at low surface concentrations ($\Gamma \approx 2 \times 10^{-12}$ mol cm^{-2}), the $t_{1/2}$ values are <20 s, but as the surface concentration increases, they increase, until leveling off in the $t_{1/2} \approx 30-50$ s range at a surface concentration of $\Gamma \approx 2 \times 10^{-11}$ mol cm^{-2}.

B. XPS Studies of the ZnPS$_n$ SAMs. The general surface characteristics of a collection of e-beam evaporated Au films deposited on Si(100) were examined by XPS prior to monolayer deposition to survey the quality of the initial substrates. Measurements on the clean surfaces revealed intense Au signals near 84, 88, 335, and 353 eV, corresponding to the $4f_{7/2}$, $4f_{5/2}$, $4d_{5/2}$, and $4d_{3/2}$ states, respectively. Weak signals were also seen from carbon and oxygen. These signals are an indication of the minor contamination of the Au surface commonly resulting from adsorption of adventitious hydrocarbons and/or water present in the ambient environment, and they point to the unreliable nature of the C 1s signal for quantitative determinations of surface concentrations.

The XPS signatures of the saturation-coverage **ZnPS$_n$** SAMs were examined to characterize the binding motif of the mono-

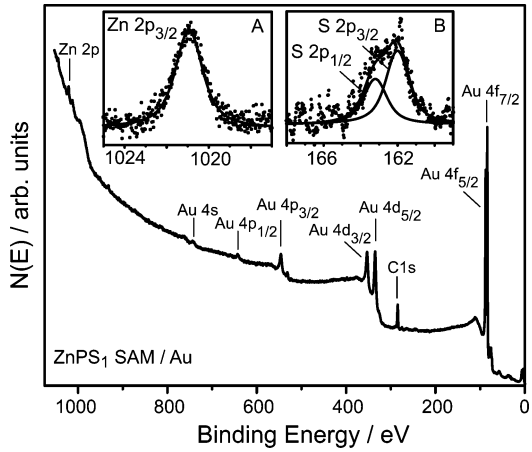

Figure 4. Survey XPS of the saturation-coverage **ZnPS$_1$** SAM on Au. Inset A: High-resolution scan of the Zn $2p_{3/2}$ spectral region, showing both the raw data (dots) and a fit (solid). Inset B: High-resolution scan of the S $2p_{3/2}$ and S $2p_{1/2}$ spectral region, raw data (dots) and fit (solid).

Table 2. Sulfur Atom Binding Energies and Atomic Ratios for Signature Elements in the **ZnPS$_n$** SAMs

	sulfur binding energy (eV)[a]		estimated atomic ratio		
	bound	unbound	S 2p:Zn $2p_{3/2}$		N:Zn
SAM	S $2p_{3/2}$	S $2p_{3/2}$	S_T[b]	S_B[b]	N 1s:Zn 2p3/2
ZnPS$_1$	162.0		0.9	0.9	3.9
cis-**ZnPS$_2$**	162.0	163.5	2.1	1	3.9
trans-**ZnPS$_2$**	162.2	163.7	1.9	0.9	4.1
ZnPS$_3$	161.9	163.7	3.0	0.9	3.8
ZnPS$_4$	162.0	163.7	3.7	0.9	3.7

[a] $\pm$0.1 eV. [b] S_T and S_B refer to the estimated total (bound + unbound) and bound sulfur, respectively.

layer to the Au surface; acquisition of XPS data for SAMs below saturation coverages was not possible because of the low signal levels obtained for the key signature elements such as S. A representative survey spectrum of the **ZnPS$_1$** SAM is shown in Figure 4. The spectra of all of the **ZnPS$_n$** SAMs exhibit multiple peaks consistent with the molecular composition of the porphyrins bearing thiol groups. In particular, in addition to signals from the bulk Au, the spectra show discrete signals for Zn, S, and N from the porphyrin. The high-resolution Zn $2p_{3/2}$ (Figure 4, inset A) and N 1s (not shown) signals are observed at binding energies of 1020.9 $\pm$ 0.1 and 398.2 $\pm$ 0.1 eV, respectively, in qualitative agreement with previously reported values for zinc porphyrins.[35,43,44] Quantitative analysis of the spectra was also carried out by scaling the spectral intensity of each element of interest (S, Zn, N) using known atomic cross-section sensitivity factors.[45] The last column of Table 2 summarizes the experimentally determined values for the N:Zn atomic ratios, which correspond well to the 4:1 (N:Zn) atomic ratio expected for the porphyrin within the 10−15% uncertainty in the spectral fits of the raw data. We note that signal attenuation due to the SAMs is negligible in these systems.

The chemical environment of the S atoms was examined in detail. Inset B of Figure 4 shows a representative high-resolution S 2p spectrum for the **ZnPS$_1$** SAM. The data could be fitted to a single set of peaks with S $2p_{3/2}$ and S $2p_{1/2}$ components

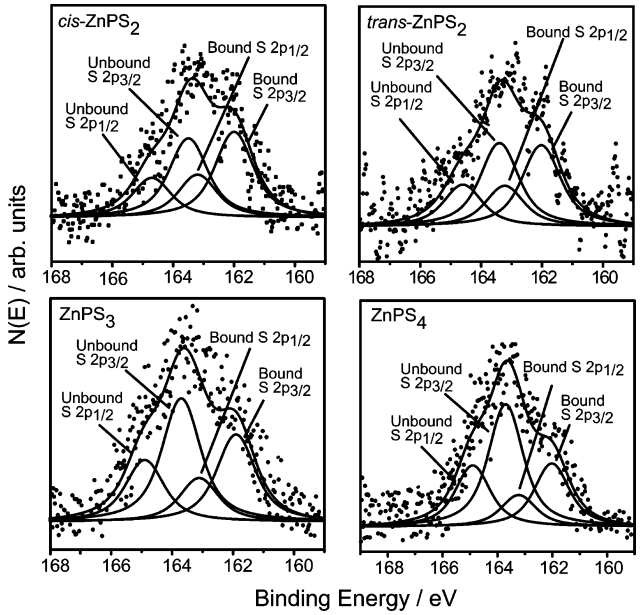

Figure 5. High-resolution XPS of the saturation-coverage **ZnPS$_n$** (n = 2−4) SAMs in the S 2p spectral region, raw data (dots) and fit (solid). Each spectrum was fitted to two sets of S $2p_{3/2}$ and S $2p_{1/2}$ peaks. The low and higher energy sets are representative of bound and unbound S, respectively (see text).

centered at binding energies of 162.0 $\pm$ 0.1 and 163.2 $\pm$ 0.1 eV, respectively. In contrast, signals from two types of sulfurs were observed for the SAMs of all of the **ZnPS$_n$** molecules containing more than one thiol (Figure 5). A list of the S $2p_{3/2}$ binding energies obtained after fitting the XPS spectrum from each of these SAMs is given in Table 2. For each of the SAMs exhibiting signals from two types of S atoms, the same two binding energy values were obtained within experimental error, 162.0 $\pm$ 0.1 and 163.7 $\pm$ 0.1 eV. This result strongly suggests that the same two types of S moieties are present in all of the SAMs. The binding energy of 162.0 eV matches that of **ZnPS$_1$** and is in generally good agreement with that observed for neat alkanethiols[46−49] and thiol-functionalized porphyrin monolayers chemisorbed onto Au substrates.[35−37] On the other hand, the binding energy of the second type of S is upshifted by ~1.5 eV from that typical of an S−Au species. Previous studies of thiol SAMs have attributed S $2p_{3/2}$ signals at these binding energies to the presence of unbound thiols.[35−37] Accordingly, all of the **ZnPS$_n$** (n = 2−4) SAMs exhibit both bound and unbound thiols.

To quantify the amount of bound versus unbound thiol in the **ZnPS$_n$** (n = 2−4) SAMs, the XPS signal intensities for the two types of S atoms were scaled against those for the Zn atom. Those data are summarized in Table 2. The table lists the S:Zn ratios obtained experimentally for both the total S content, S_T, and the bound S content, S_B. The S_T ratio reflects the stoichiometry expected from the molecular structure, whereas the S_B ratio reflects the fraction of S atoms bound to the Au surface. The S_T ratios obtained experimentally are in good agreement

(44) Polzonetti, G.; Ferri, A.; Russo, M. V.; Iucci, G.; Licoccia, S.; Paolesse, R. *J. Vac. Sci. Technol., A* **1999**, *17*, 832−839.
(45) *Handbook of X-ray Photoelectron Spectroscopy*; Wagner, C. D., Riggs, W. M., Davis, L. E., Moulder, J. F., Muilenberg, G. E., Eds.; Perkin-Elmer Corp.: Eden Prairie, 1978.
(46) Laibinis, P. E.; Whitesides, G. M.; Allara, D. L.; Tao, Y.-T.; Parikh, A. N.; Nuzzo, R. G. *J. Am. Chem. Soc.* **1991**, *113*, 7152−7167.
(47) Weisshaar, D. E.; Walczak, M. M.; Porter, M. D. *Langmuir* **1993**, *9*, 323−329.
(48) Nuzzo, R. G.; Zegarski, B. R.; Dubois, L. H. *J. Am. Chem. Soc.* **1987**, *109*, 733−740.
(49) Bain, C. D.; Biebuyck, H. A.; Whitesides, G. M. *Langmuir* **1989**, *5*, 723−727.

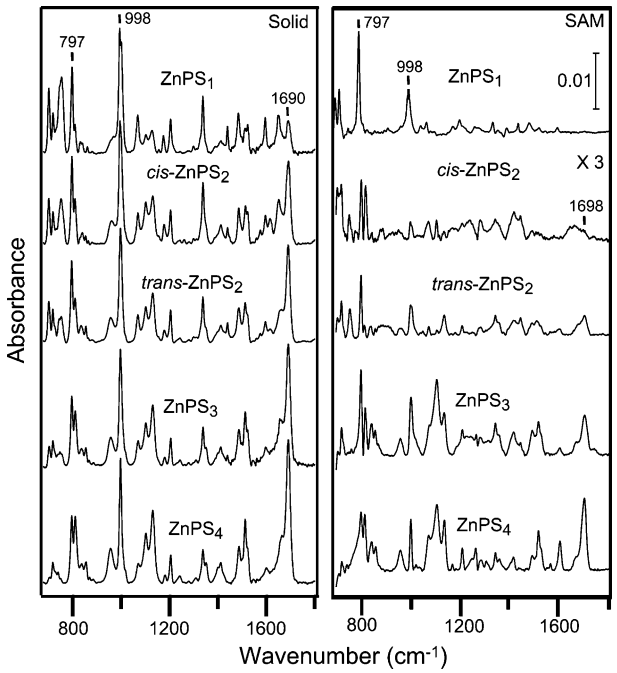

Figure 6. FTIR spectra of the **ZnPS$_n$** ($n = 1-4$) solids (left panel) and in saturation-coverage SAMs (right panel).

with those expected on the basis of the structures of the molecules, from one to four according to the value of n in **ZnPS$_n$** ($n = 1-4$). On the other hand, the S_B ratio was measured to be approximately unity for all of the multithiol porphyrin SAMs. This implies that each of the porphyrins studied at its respective saturation surface concentration is anchored through a single Au−S bond.

C. FTIR Studies of the ZnPS$_n$ SAMs. The mid-frequency (680−1800 cm^{-1}) IR spectra of solid samples of the **ZnPS$_n$** molecules are shown in Figure 6 (left panel). The spectra exhibit numerous bands in this frequency region. Previous studies of structurally related porphyrins have shown that the majority of these bands are due to in-plane modes of the porphyrin ring or the aryl substituents, one of the most prominent features being the porphyrin pyrrole ring breathing mode near 998 cm^{-1}.[50] The only prominent feature that is due to an out-of-plane mode of the porphyrin is the band at 797 cm^{-1}, which is due to a β-pyrrole hydrogen deformation.[51] For the **ZnPS$_n$** molecules, another important band relevant to this work is that at 1690 cm^{-1}, which is assigned to the carbonyl stretching vibration(s) ν(C═O) of the *S*-acetyl protecting group(s).[13] The intensity of this latter band generally increases (relative to the porphyrin bands) as the number of ***S*-AcSCH$_2$pep** appendages increases. In the high-frequency (2600−3400 cm^{-1}) spectral region (not shown), only weak bands are observed, all attributable to C−H stretches.

The mid-frequency (680−1800 cm^{-1}) IR spectra of the saturation-coverage **ZnPS$_n$** SAMs are also shown in Figure 6 (right panel). The spectra of all of the **ZnPS$_n$** SAMs are plotted on the same absolute intensity scale to compare the relative intensities of the bands, although the spectrum for the *cis*-**ZnPS$_2$** SAM is shown on an expanded intensity scale to facilitate the viewing of its weak bands. The key features observed in the IR spectra of the SAMs are summarized below.

(1) Comparison of the SAM and solid spectra of **ZnPS$_1$**, *trans*-**ZnPS$_2$**, **ZnPS$_3$**, and **ZnPS$_4$** reveals that the frequencies of the IR bands of each pair are similar. This result indicates that the structure of the porphyrin macrocycle and substituent groups is retained upon SAM formation. Note, however, that the frequency of the ν(C═O) mode is slightly higher in the SAMs (1698 cm^{-1}) than in the solid (1690 cm^{-1}). In the case of *cis*-**ZnPS$_2$**, all of the bands are quite weak, partially due to the low saturation coverage (vide supra), and the similarities between the solid and SAM spectra are more difficult to assess. Nevertheless, the bands due to the in-plane pyrrole breathing (998 cm^{-1}) and out-of-plane β-hydrogen deformation (797 cm^{-1}) modes are still apparent in the spectrum of the *cis*-**ZnPS$_2$** SAM, at the same values as for the solid, suggesting that the structure of this molecule is also unaltered upon SAM formation.

(2) For the **ZnPS$_1$** SAM, there is no evidence of a ν(C═O) vibration at 1698 cm^{-1} due to the acetyl protecting group, consistent with cleavage of this group upon SAM formation. On the other hand, each of the four porphyrins that contain multiple ***S*-AcSCH$_2$pep** appendages exhibits some intensity for the ν(C═O) vibration. This observation indicates that the upshifted signal of the unbound S atom seen in XPS is due to an uncleaved, protected thiol, not to some other type of thiol that has been altered by SAM formation or any interaction with the surface. In the case of the *cis*-**ZnPS$_2$** SAM, the intensity of the ν(C═O) band relative to the porphyrin bands is lower than is observed for the *trans*-**ZnPS$_2$** SAM, whereas the intensities of the XPS signals for the bound and unbound thiols are similar for the two types of SAMs. As will be discussed below, this is likely due to a difference in the orientation of the *S*-acetyl group with respect to the Au surface.

(3) There are certain differences in the absolute IR intensities of the SAMs among the different **ZnPS$_n$** molecules. For instance, the *cis*-**ZnPS$_2$** SAM clearly exhibits lower absolute IR intensities for all vibrational bands than any of the other four SAMs. This result is qualitatively consistent with the electrochemical studies, which indicate that the saturation surface concentration for the *cis*-**ZnPS$_2$** SAM is significantly lower than for the other **ZnPS$_n$** SAMs (see Table 1). We also note that the IR intensities for the **ZnPS$_1$** and *trans*-**ZnPS$_2$** SAMs appear to be somewhat lower than those of the **ZnPS$_3$** and **ZnPS$_4$** SAMs. However, these differences cannot be related in a straightforward manner to differences in saturation coverage exclusively because orientation effects also strongly influence the appearance of the IR spectra. This point will be discussed further below.

(4) There are differences in the relative IR intensities of the in-plane (e.g., 998 cm^{-1}) versus out-of-plane (797 cm^{-1}) porphyrin modes among different members of the **ZnPS$_n$** series. In particular, the IR intensities for the in-plane modes relative to the out-of-plane mode of **ZnPS$_1$** and *cis*-**ZnPS$_2$** SAMs are smaller than those of the **ZnPS$_3$** and **ZnPS$_4$** SAMs, with *trans*-**ZnPS$_2$** SAM being somewhere in between. This effect, in conjunction with the fact that in-plane modes dominate the IR spectra, is largely responsible for the large apparent differences in the absolute IR intensities of **ZnPS$_1$** and *trans*-**ZnPS$_2$** versus **ZnPS$_3$** and **ZnPS$_4$**. The relative intensities of the in-plane and out-of-plane modes of the porphyrins in the SAM are influenced

(50) Li, X. Y.; Czernuszewicz, R. S.; Kincaid, J. R.; Su, Y. O.; Spiro, T. G. *J. Phys. Chem.* **1990**, *94*, 31−47.
(51) Li, X. Y.; Czernuszewicz, R. S.; Kincaid, J. R.; Spiro, T. G. *J. Am. Chem. Soc.* **1989**, *111*, 7012−7023.

by the orientation of the molecule with respect to the plane of the surface because only the components of the transition moments of the vibrations of molecules adsorbed on metals perpendicular to the plane of the surface contribute to the IR intensities.[52] The IR intensity increases monotonically as the transition moment rotates out-of-plane and disappears when the transition moment is parallel to the surface.[53]

The relative intensities of the in-plane and out-of-plane porphyrin modes can be used to determine the average tilt angle (α) of the porphyrin ring with respect to the surface normal. The evaluation of the average tilt angle is predicated on certain assumptions. (1) The porphyrin ring is planar, and thus the 998 and 797 cm^{-1} modes are pure in-plane and out-of-plane vibrations, respectively. This assumption is reasonable considering that Zn tetraphenylporphyrin is planar.[54] (2) The intrinsic transition-dipole moments of the porphyrin vibrations in the randomly oriented solid phase and in the surface-bound monolayer are the same. (3) The orientation of the porphyrin ring can be described by one single angle, the average tilt from the surface normal. Two more angles are in principle needed to fully determine adsorption geometries, the polar angle around the surface normal (assumed here to be random), and the rotation around the main molecular axis (fixed at 0° with respect to the surface plane). Preliminary work in our lab suggests that this angle may vary from 0°, but that this variation may not affect much the estimate of the azimuthal angle reported below. Under these assumptions, the average azimuthal tilt angle for the porphyrins in the SAMs can be determined from the ratios of the relative intensities of the in-plane and out-of-plane porphyrin modes in the SAMs versus the solids using standard methods.[52,53] The angles determined from the IR data for the saturation-coverage **ZnPS$_n$** SAMs are as follows: **ZnPS$_1$**, $\alpha \approx 58°$; *cis*-**ZnPS$_2$**, $\alpha \approx 58°$; *trans*-**ZnPS$_2$**, $\alpha \approx 50°$; **ZnPS$_3$**, $\alpha \approx 47°$; **ZnPS$_4$**, $\alpha \approx 44°$.

The average tilt angle for the porphyrins in the **ZnPS$_n$** SAMs, together with the number and position of the ***S*-AcSCH$_2$pep** appendages, determine the molecular footprint on the surface. Accordingly, the more upright orientation for the molecules in the **ZnPS$_3$** and **ZnPS$_4$** SAMs is likely a contributing factor to the higher saturation surface concentrations observed for these SAMs versus the more tilted *cis*-**ZnPS$_2$** and *trans*-**ZnPS$_2$** SAMs. The more tilted orientation of *cis*-**ZnPS$_2$** versus *trans*-**ZnPS$_2$** may also result in the C═O transition dipole of the *S*-acetyl group of the former molecule being more parallel to the surface plane than that of the latter, leading to its attenuated IR intensity (relative to the porphyrin modes). On the other hand, the **ZnPS$_1$** SAMs exhibit relatively high saturation surface concentrations despite a more tilted orientation. This result is likely due to the fact that the phenyl substituents are small relative to the ***S*-AcSCH$_2$pep** appendages of the other molecules.

To evaluate more fully the effects of surface concentration on porphyrin orientation, FTIR spectra were obtained for the **ZnPS$_1$** and **ZnPS$_4$** SAMs as a function of surface coverage. These two SAMs were chosen for this study for two reasons. (1) Both porphyrins can attain high surface coverage and therefore provide a good dynamic range over which the IR data could be obtained. (2) These two porphyrins are the most different in their nonbinding substituent groups. The IR spectra of **ZnPS$_1$** and **ZnPS$_4$** SAMs as a function of surface concentration are shown in Figure 7, left and right panels, respectively. The surface concentrations range from the low 10^{-11} mol cm^{-2} range (the lowest concentrations detectable by IR) to saturation. The surface concentrations and average tilt angles are noted on the individual spectra.

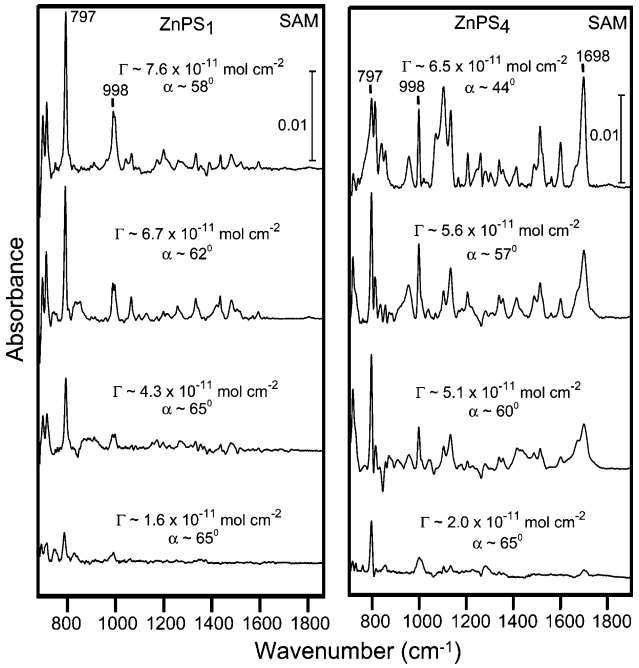

Figure 7. FTIR spectra of the **ZnPS$_1$** (left panel) and **ZnPS$_4$** (right panel) SAMs at various surface concentrations. The surface concentrations and the average tilt angles are indicated above each spectrum.

Inspection of the data shown in Figure 7 reveals the following trends. (1) For both the **ZnPS$_1$** and **ZnPS$_4$** SAMs, the tilt angle increases as the surface concentration decreases from the saturation value. (2) The change in average tilt angle for the **ZnPS$_1$** SAM is much smaller (~7°) than that for the **ZnPS$_4$** SAM (~21°). (3) The average tilt angles for both types of SAMs appear to converge to a similar value of $\alpha \approx 65°$ at surface concentrations near $\Gamma \approx 4 \times 10^{-11}$ mol cm^{-2}, which is only modestly below the saturation value ($\Gamma \approx 7 \times 10^{-11}$ mol cm^{-2}). (4) For **ZnPS$_4$**, no abrupt intensity change occurs for the ν(C═O) band as the surface concentration decreases. If such an intensity change were observed, it could imply binding via a second thiol as the porphyrins become sparse on the surface. Finally, we note that the trend in average tilt angles as a function of surface concentration observed for the **ZnPS$_1$** and **ZnPS$_4$** SAMs qualitatively parallels the trend observed in the redox thermodynamic parameters. In particular, for the **ZnPS$_1$** SAM, both $E^{0/+1}$ and $\Delta E_{p,1/2}$ exhibit only modest changes in value over the concentration range $\Gamma \approx 1-7 \times 10^{-11}$ mol cm^{-2}, whereas for the **ZnPS$_4$** SAM, the changes in these redox parameters are much larger (see Figure 2).

IV. Discussion

The studies reported herein on the series of **ZnPS$_n$** SAMs permit a systematic exploration of the factors that influence (1) the binding mode of the SAMs to the Au surface, (2) the orientation of the porphyrin rings with respect to the surface

(52) Greenler, R. G. *J. Chem. Phys.* **1966**, *44*, 310−315.
(53) Yates, J. T., Jr.; Madey, T. E.; Eds. *Vibrational Spectroscopy of Molecules on Surfaces*; Plenum Press: New York, 1987.
(54) Scheidt, W. R.; Kastner, M. E.; Hatano, K. *Inorg. Chem.* **1978**, *17*, 706−710.

plane, and (3) the packing density of the adsorbed layer. These structural properties of the SAMs underpin the thermodynamics and kinetics of electron transfer. In the sections below, we address each of these issues.

The first general theme that emerges from our studies is that, regardless of the number of ***S*-AcSCH$_2$pep** appendages available for binding to the Au surface, binding only occurs through a single linkage (at saturation coverage). Moreover, in the SAMs of the multithiol-functionalized porphyrins, the unbound thiols retain their acetyl protecting groups. This latter observation implies that the unbound thiols either never make contact with the Au surface or that the contact time is too short to cause cleavage of the protecting group. This explanation seems unlikely, however, given that attachment via multiple thiols is not seen on the surface even at low coverages (Figure 7).

The fact that a molecule such as *trans*-**ZnPS$_2$** does not bind via both thiols is not surprising given that attachment in this fashion would require that the porphyrin lie completely flat on the surface. This geometry is precluded because the aryl substituents on the *meso*-positions of the porphyrin are not coplanar with the porphyrin macrocycle (due to steric constraints),[54] thereby restricting access of the second thiol to the surface. Indeed, the ***S*-AcSCH$_2$pep** appendage was specifically chosen to disfavor surface geometries in which the porphyrin ring lies (nearly) flat on the surface. Perhaps more surprising is the observation that none of the **ZnPS$_n$** molecules that contain *cis*-thiol-functionalization bind via a pair of adjacent thiols, because in those cases, the ***S*-AcSCH$_2$pep** appendage does not impose any steric constraints to preclude binding via two adjacent thiols. In addition, the presence of the methylene group in the ***S*-AcSCH$_2$pep** appendage places the thiol moiety at the end of a conformationally flexible tether. One explanation for the failure of the second thiol to bind to the surface is that the free energy associated with packing of the disklike porphyrin molecules outweighs any additional thermodynamic stabilization afforded by the formation of a second Au−S bond. In this regard, changes in adsorption geometry from lying flat to tilted upon increasing packing are common with aromatic molecules on metal surfaces.[55,56] Alternatively, the kinetics of the deposition process may also come into play in these systems. In particular, multiple porphyrins may arrive simultaneously in the same vicinity and begin to pack as they bind, blocking adjacent sites and therefore precluding attachment of the second *cis*-thiol. Note, however, that if this latter effect does indeed influence the binding mode, then it must come into play even when the SAMs are at less than saturation coverage. We further note that binding by two adjacent thiols cannot be completely ruled out at very low surface coverage (10^{-12} mol cm^{-2} range), because the spectroscopic tools available do not have sufficient sensitivity to interrogate the SAMs at these surface concentrations.

The second observation derived from this work is that the orientation and packing density of the **ZnPS$_n$** molecules on the surface are strongly influenced by the nature (***S*-AcSCH$_2$pep** versus phenyl groups), position (cis versus trans), and number of the substituent groups. In particular, at saturation coverage, the porphyrins in the **ZnPS$_1$** and *cis*-**ZnPS$_2$** SAMs are more tilted ($\alpha \approx 58°$) with respect to the surface normal than those in the **ZnPS$_3$** and **ZnPS$_4$** SAMs ($\alpha \approx 44°$). The tilt angle of the porphyrins in the *trans*-**ZnPS$_2$** SAM ($\alpha \approx 50°$) is intermediate between these two values. The less tilted orientation for the porphyrins in the **ZnPS$_3$** and **ZnPS$_4$** allows these molecules to pack more tightly than the porphyrins in the *cis*-**ZnPS$_2$** or *trans*-**ZnPS$_2$** SAMs. Indeed, the molecular areas for the porphyrins in the **ZnPS$_3$** and **ZnPS$_4$** SAMs are comparable to those of the **ZnPS$_1$** SAM (see Table 2), despite the fact that the multiple ***S*-AcSCH$_2$pep** appendages of the former molecules are much larger than the phenyl groups of the latter.

The observation that the more bulky porphyrins in the **ZnPS$_3$** and **ZnPS$_4$** SAMs can pack more tightly than the other members of the set seems counterintuitive. We do not have a complete explanation for this observation and can only speculate why this trend is observed. Interactions between the ***S*-AcSCH$_2$pep** appendages on neighboring molecules must play a large role in determining the packing. In particular, for the **ZnPS$_3$** and **ZnPS$_4$** SAMs, there are two ***S*-AcSCH$_2$pep** appendages adjacent to the **SCH$_2$pep** linker to the surface. [In the case of **ZnPS$_3$**, we speculate that this is the preferred binding geometry, as opposed to asymmetrical binding resulting in one adjacent and one opposite ***S*-AcSCH$_2$pep** appendage.] Possibly, the terminal ethynylphenyl portion of these adjacent ***S*-AcSCH$_2$pep** appendages can π stack with the porphyrin macrocycle of a neighboring molecule. This type of packing would seem to be the only way that the porphyrins in the **ZnPS$_3$** and **ZnPS$_4$** SAMs could achieve packing densities and effective molecular areas approaching those exhibited by the porphyrins in the **ZnPS$_1$** SAM. On the other hand, this type of $\pi-\pi$ interaction is not possible for the ***S*-AcSCH$_2$pep** appendage opposite to the linker to the surface. This might explain why the porphyrins in the *trans*-**ZnPS$_2$** SAM are more tilted and less tightly packed than those in the **ZnPS$_3$** and **ZnPS$_4$** SAMs. It should be noted, however, that if $\pi-\pi$ stacking does drive the packing of the latter SAMs, one might speculate that the *cis*-**ZnPS$_2$** SAM would also be tightly packed, rather than loosely as is observed. The poor packing of the *cis*-**ZnPS$_2$** SAM might be explained by the asymmetric substituent pattern (***S*-AcSCH$_2$pep** and phenyl) of the groups that are adjacent to the linker to the surface. Achieving long range $\pi-\pi$ stacking between the single ***S*-AcSCH$_2$pep** appendage and a neighboring porphyrin would require an arrangement of porphyrins on the surface that is entropically unfavorable.

The third conclusion arising from the studies reported herein is that the packing density influences both the thermodynamics and the kinetics of electron transfer. All of the **ZnPS$_n$** SAMs follow the same general trend as the surface concentration increases. As the monolayers become more densely packed, the redox process becomes less favorable, more heterogeneous, and slower (see Figures 2 and 3). The largest effects are observed at the lowest surface concentrations ($\Gamma < 1 \times 10^{-11}$ mol cm^{-2}). Interestingly, changes in the average tilt angle of the porphyrin as a function of surface concentration appear to be correlated with changes in the redox thermodynamics, but not the kinetics (cf. Figure 7 with Figures 2 and 3). We are uncertain as to why the thermodynamics and kinetics are affected differently. Regardless, the influence of surface concentration on the redox thermodynamics and kinetics is likely due to space-charge effects.[25] The space charge on the SAM increases as the surface

(55) Zaera, F. *Prog. Surf. Sci.* **2001**, *69*, 1−98.
(56) Netzer, F. P.; Ramsey, M. G. *Crit. Rev. Solid State Mater. Sci.* **1992**, *17*, 397−475.

concentration increases. Space-charge effects are exacerbated in very densely packed monolayers because the solvent/counterions have more limited access to the redox center.

The observation that the electron-transfer kinetics exhibit only small changes in surface-concentration regimes where the average tilt angle (and the distance) of the porphyrin with respect to the surface is changing the most (i.e., $\Gamma > \sim 4 \times 10^{-11}$ mol cm^{-2}) has implications for the mechanism of electron transfer. In particular, this observation argues against any significant though-space contribution to the electron-transfer process, at least in that surface concentration range, because changes in the distance of the redox center to the surface would be expected to strongly affect the rates if this mechanism were operative. Instead, the results are more consistent with the notion that the dominant mechanism for electron transfer from the porphyrin to the surface is a through-bond nonadiabatic process that involves the **SCH$_2$pep** linker as a superexchange mediator, as suggested by previous studies.[23−25] In this regard, the fact that the porphyrins in all of the **ZnPS$_n$** SAMs in the high coverage regime are linked to the surface via a single thiol would result in a similar linker-mediated electronic coupling between the molecule and the surface.

V. Outlook

The studies reported herein to elucidate the structural features of the **ZnPS$_n$** SAMs have implications that extend beyond our immediate investigation of porphyrins for information-storage applications. In particular, the studies show that the surface orientation and packing density of the **ZnPS$_n$** SAMs can be controlled by the number and position of the ***S*-AcSCH$_2$pep** appendages. However, the surface binding mode, orientation, and packing density in the SAMs are determined by a complex interplay of intra- and intermolecular forces. Our seemingly reasonable preconceived notion concerning how the position of potential surface binding groups (*cis*-thiol designs) would affect binding did not prove correct. Similarly, the number and placement of the ***S*-AcSCH$_2$pep** appendages have a much larger effect on the orientation and packing density of the molecules than might have been expected. Indeed, the presence of multiple, accessible surface attachment groups does not imply binding of multiple groups upon SAM formation. Collectively, these observations point to the difficulty of predicting the structure of SAMs on the basis of the structure of the component molecules alone. In this respect, predictions of the structure of the porphyrin SAMs appear to have many of the same challenges associated with crystal engineering, where the overall architecture is dictated by the sum of a large number of subtle molecular interactions.

Acknowledgment. This work was supported by the Center for Nanoscience Innovation for Defense and DARPA/DMEA (under award number DMEA90-02-2-216) and Zettacore. We thank J. Diers for obtaining the solution electrochemical data. Mass spectra were obtained at the Mass Spectrometry Laboratory for Biotechnology at North Carolina State University. Partial funding for the facility was obtained from the North Carolina Biotechnology Center and the NSF.

Supporting Information Available: Complete synthetic procedures and spectral data for each new compound. This material is available free of charge via the Internet at http://pubs.acs.org.

JA047723T